Molecular Crystals and Liquid Crystals Science and Technology. Section A. Molecular Crystals and Liquid Crystals

Publication details, including instructions for authors and subscription information:
http://www.tandfonline.com/loi/gmcl19

DYNAMICAL SIMULATION OF ORIENTATION TEXTURE EVOLUTION OF A POLYMERIC LIQUID CRYSTAL UNDER SIMPLE SHEAR FLOW

W. H. Han [a] , S. T. Koh [a] , S. G. Noh [a] , J. K. Jeon [a] & J. H. Cho [a]

[a] Department of Chemical Engineering, Dong Yang University Kyochondong, 1-bunjee, Young Jou city, Kyungbook, 750-711, Korea

Version of record first published: 24 Sep 2006

To cite this article: W. H. Han, S. T. Koh, S. G. Noh, J. K. Jeon & J. H. Cho (2001): DYNAMICAL SIMULATION OF ORIENTATION TEXTURE EVOLUTION OF A POLYMERIC LIQUID CRYSTAL UNDER SIMPLE SHEAR FLOW, Molecular Crystals and Liquid Crystals Science and Technology. Section A. Molecular Crystals and Liquid Crystals, 366:1, 929-936

To link to this article: http://dx.doi.org/10.1080/10587250108024036

Mol. Cryst. and Liq. Cryst., 2001, Vol. 366, pp. 929-936
Reprints available directly from the publisher
Photocopying permitted by license only

Dynamical Simulation of Orientation Texture Evolution of a Polymeric Liquid Crystal under Simple Shear Flow

W.H. HAN, S.T. KOH, S.G. NOH, J.K. JEON and J.H. CHO

Department of Chemical Engineering, Dong Yang University Kyochondong 1-bunjee, Young Jou city, Kyungbook 750-711 Korea

Dynamical simulation of orientation texture evolution of a polymeric liquid crystal under simple shear flow has been carried out. The Leslie-Ericksen equation was numerically solved to obtain three dimensional orientation over the shear plane spanned by the flow (x) and thickenss (y) axes. The present study shows a cascade of complex orientation texture evolutions as a function of the Ericksen number (E) during shear flow starting from a near perfect monodomain condition. When $E_2>E>E_1$, directors in the middle gap region twist out of the shear plane in a uniform sense. When $E_3>E>E_2$, the twist sense is not of the same sign, but alternating along the flow axis. When $E_4>E>E_3$, the middle orientation wall of the alternating twist sense divides into a pair, which migrate towards the bounding plates, forming a series of tubular orientation walls. When $E>E_4$, the tubular orientation walls still form, but through a reentrant two-dimensional in-shear-plane state.

Keywords: Nematodynamics; Polymeric Liquid Crystals; Leslie-Ericksen Theory; Shear Flow; Pattern Formation

INTRODUCTION

For the last half century, light transmission patterns of sheared liquid crystalline polymers under crossed polars have frequently been reported in the literature, known as the banded texture[1,2,3,4,5,6] which now serves as a fingerprint of the polymeric liquid crystal phase. Experimental studies[2,3,4,5,6] have established that the banded texture is a result of some periodic spatial undulation of the orientation or the effective birefringence. The banded texture can be frozen-in, and correlations

between the banded texture and anisotropic mechanical properties[7] indicate the importance of fundamental study of this phenomenon.

Taking account of the orientation gradients along both the thickness and the flow directions, a numerical simulation of shear flow of a liquid crystalline polymer using the Leslie-Ericksen equation has given a plausible explanation of the banded texture[8]; polarized light transmission calculation using the computed orientation field gave the experimentally observed undulating pattern along the flow direction. The computed orientation profile showed a complex three-dimensional orientation texture, which is characterized by a series of tubular orientation walls in the shear plane spanned by the flow and the thickness axes. The present contribution further investigates the orientation texture evolutions towards the tubular orientation walls formation.

THEORY AND SOLUTION METHOD

The Leslie-Ericksen(L-E) theory consists of the linear momentum balance and the torque balance of the unit vector $\mathbf{n}$, director, representing the local orientation[9]. The linear momentum balance is given by :

$$\rho \dot{\boldsymbol{v}} = \mathbf{f} + \nabla \cdot \boldsymbol{\sigma} \tag{1}$$

where ρ, $\boldsymbol{v}$, $\mathbf{f}$ and $\boldsymbol{\sigma}$ are the density, velocity, body force per unit volume and total stress, respectively. The superposed dot denotes the material time derivative. The total stress tensor $\boldsymbol{\sigma}$ is given by

$$\begin{aligned}\boldsymbol{\sigma} = -p\boldsymbol{\delta} - \frac{\partial F}{(\partial \nabla \mathbf{n})^T} \cdot \nabla \mathbf{n} + \alpha_1 (\mathbf{nn} : \mathbf{A})\mathbf{nn} + \alpha_2 \mathbf{nN} \\ + \alpha_3 \mathbf{Nn} + \alpha_4 \mathbf{A} + \alpha_5 \mathbf{nn} \cdot \mathbf{A} + \alpha_6 \mathbf{A} \cdot \mathbf{nn}\end{aligned} \tag{2}$$

where p, $\boldsymbol{\delta}$, α_i (i=1,...,6), $\mathbf{A}$ and $\mathbf{N}$ are the pressure, unit tensor, Leslie viscosity coefficients, rate of deformation tensor, and corrotational time derivative of $\mathbf{n}$, respectively. The rate of deformation tensor $\mathbf{A}$ and the corrotational time derivative of the director $\mathbf{N}$ are given by

$$2\mathbf{A} = (\nabla \boldsymbol{v} + (\nabla \boldsymbol{v})^T), \qquad \mathbf{N} = \dot{\mathbf{n}} - \boldsymbol{\omega} \cdot \mathbf{n} \tag{3}$$

where the rate of rotation tensor $\boldsymbol{\omega}$ is

$$2\boldsymbol{\omega} = (\nabla \boldsymbol{v} - (\nabla \boldsymbol{v})^T). \tag{4}$$

The torque balance is given by

$$0 = \boldsymbol{\Gamma}^v + \boldsymbol{\Gamma}^e, \tag{5}$$

where the viscous torque $\mathbf{\Gamma}^v$ and the elastic torque $\mathbf{\Gamma}^e$ are given by:

$$\mathbf{\Gamma}^v = -\mathbf{n}\times(\gamma_1\mathbf{N} + \gamma_2\mathbf{A}\cdot\mathbf{n}), \tag{6}$$

$$\mathbf{\Gamma}^e = -\mathbf{n}\times(\frac{\partial F}{\partial \mathbf{n}} - \nabla\cdot\frac{\partial F}{\partial(\nabla\mathbf{n})^T}) \tag{7}$$

where γ_1 and γ_2 are the rotational and irrotational viscosities, respectively[10]. The Frank orientation curvature elastic energy F is given by:

$$2F = K_{11}(\nabla\cdot\mathbf{n})^2 + K_{22}(\mathbf{n}\cdot\nabla\times\mathbf{n})^2 + K_{33}\mid\mathbf{n}\times\nabla\times\mathbf{n}\mid^2 \tag{8}$$

where K_{11}, K_{22}, and K_{33} are the splay, twist and bend constants, respectively. The orientation behavior during flow is controlled by the Ericksen number $\mathcal{E}$, a characteristic ratio between the viscous and elastic torques, given by

$$\mathcal{E} = \gamma_1\dot{\gamma}h^2/\left(\prod_{i=1}^{3}K_{ii}\right)^{1/3} \tag{9}$$

where $\dot{\gamma}$ and $h(=3.5\times10^{-4}m)$ denote the apparent shear rate and the gap thickness, respectively. The experimentally measured material constants are (γ_1,γ_2)= (6.938, −6.902) Pa·s and (K_{11}, K_{22}, K_{33}) =(1.21, 0.078, 0.763) $\times\ 10^{-11}$N [11].

The Galerkin finite element method and a fully implicit time integration method were used with 60 by 60 quadrilateral bilinear elements to obtain the director field, $\mathbf{n}$=(n_x(x,y,t), n_y(x,y,t), n_z(x,y,t)) under simple shear flow kinematics $\mathbf{v}$=($\dot{\gamma}y\Phi(t), 0, 0$)) where Φ is the Heavyside step function. The full detailed equations are found in [12]. At t=0, the uniform homeotropic director field is randomly perturbed with a maximum perturbation δn_i^2=10^{-4}, $i = x, y, z$. The fixed homeotropic anchoring boundary condition is used ($\mathbf{n}$=(0,1,0) at y=0 and h). To minimize the inlet and outlet end effects of finite length computational domain, a large aspect ratio (length/thickness) of 16 was used. At the inlet and outlet, vanishing contact torque condition was used.

RESULTS AND DISCUSSION

Figure 1 shows that when E_2>E>E_1 ($E_1\approx2130$, $E_2\approx2240$), the director orientation monotonically twist out of the shear plane spanned by the flow axis (x) and the thickness axis (y), giving rise to a non zero n_z or the non-planar orientation state. At first, the director field starts

the evolution from the initial condition shown in Figure 1(a) where the monodomain texture with homeotropic anchoring (n_x=0, n_y=1, n_z=0) is shown with medium gray color. Figure 1(i) shows a steady state orientation texture in which the director orientation of monotonic twist out of the shear plane is represented with bright gray color (n_z>0) stripe in

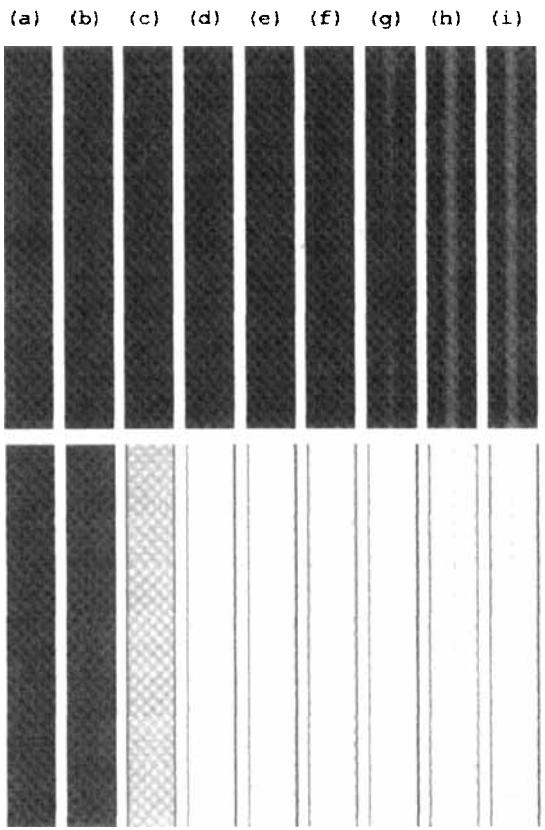

FIGURE 1. Texture evolutions of n_z(top row) and n_x(bottom row) for E=2217. Each rectangle represents a director field at time t between two parallel plates with the righthand side plate moving north. Black color means n_i=−1, white n_i=+1, medium gray n_i=0. Time(sec) for each rectangle is: (a)0.1, (b) 9.8, (c) 113, (d)580, (e)3726, (f)47900, (g)239500, (h)338900, and (i)1536000.

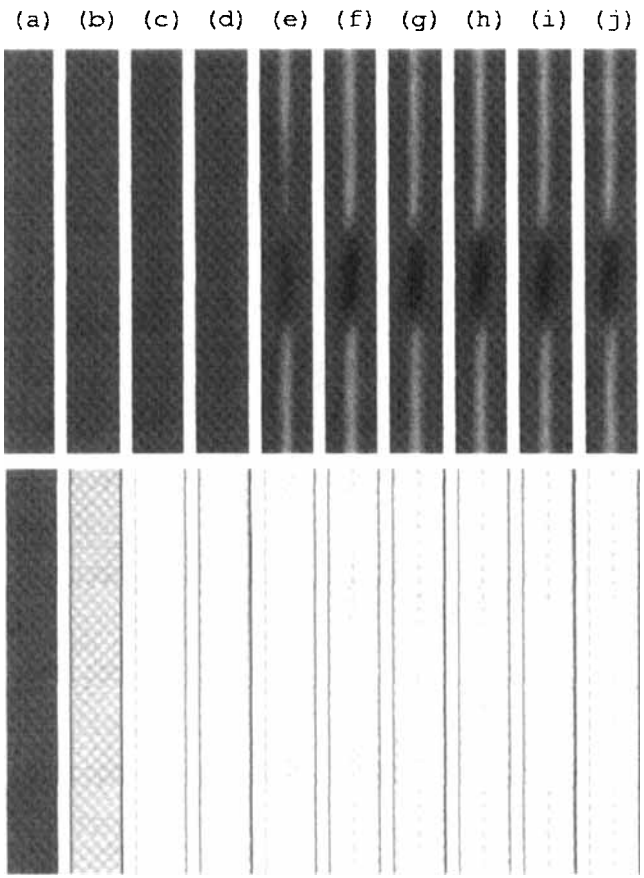

FIGURE 2. Texture evolutions of n_z(top) and n_x(bottom) for E=2276. All the conventions used in this figure are the same as in the Figure 1. Time(sec) for each rectangle is: (a)0.1, (b)113, (c)3726, (d)39050 (e) 66710, (f) 89490, (g)141200, (h)417300, (i) 2049000, (j)2465000.

the mid gap region. The corresponding bottom n_x plot shows two white color stripes sandwitching a light gray color stripe, which indicates that the directors near the bounding plates are still close to the shear plane due to the homeotropic anchoring condition; the directors orient close to the flow direction ($n_x \approx +1$) which is represented as white color.

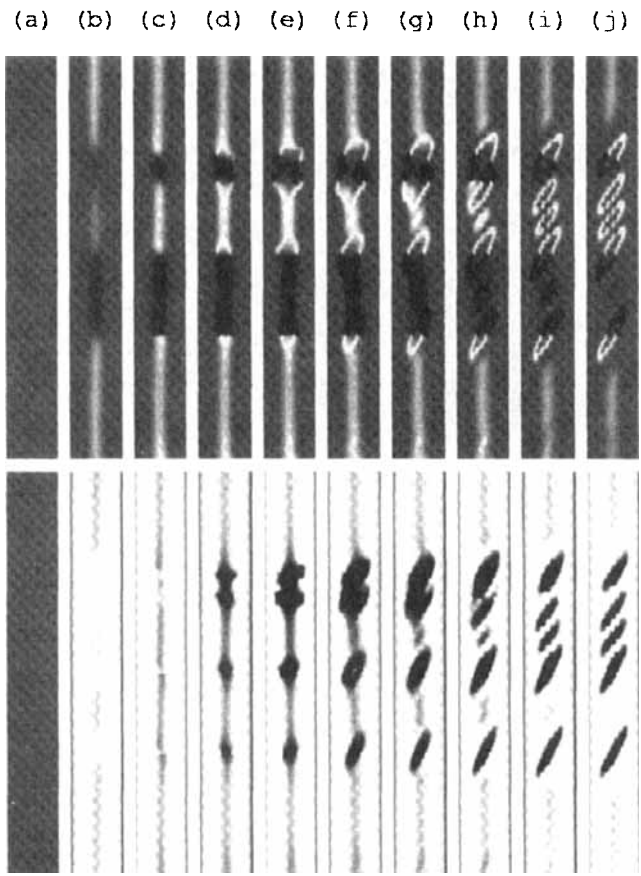

FIGURE 3. Texture evolutions of n_z(top) and n_x(bottom) for E=2305. All the conventions used in this figure are the same as in the Figure 1. Time(sec) for each rectangle is: (a)0.1, (b)44800, (c)46190, (d)46790 (e) 47460, (f) 48650, (g)49540, (h)514400, (i) 56390, (j)62960.

Figure 2 shows that when $E_3>E>E_2$ ($E_3\approx2290$), the director twist out of the shear plane is not of the same sign along the flow direction as shown in the stripe consisting of weak dark color (negative twist, $n_z<0$) and weak white color(positive twist, $n_z>0$) at steady state.

Figure 3 shows that when $E_4>E>E_3$ ($E_4\approx2500$), the director

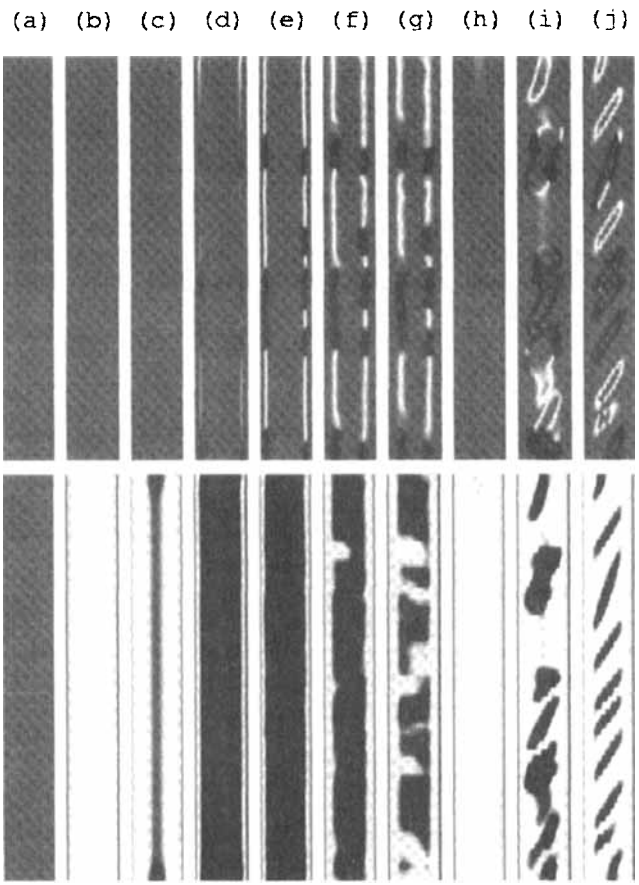

FIGURE 4. Texture evolutions of n_z and n_x for E=2627. All the conventions used in this figure are the same as in the Figure 1. Time(sec) for each rectangle is: (a)0.1, (b)3292, (c)9374, (d)10100 (e) 11120, (f) 12800, (g)13200, (h)13530, (i) 22510, (j)546000.

orientation field seems like to follow the trend shown in figure 2, but the stripe with black and white colors representing an orientation wall shown in Figure 3(b) starts dividing into a pair migrating towards the bounding plates. Some two-dimensional in-shear-plane orientation (n_z=0, planar orientation) region is created between the pair of the orientation walls

($n_z = \pm 1$). The planar orientation region is enclosed by pinching of the once divided pair of the orientation walls.

Figure 4 shows that when $E > E_4$ non-planar orientation region does not appear in the mid gap area. Instead, it appears as a pair near the bounding plates as clearly shown in stripes in Figure 4(e). The pair cannot be pinched together to enclose the planar orientation area between them. As Figure 4(h) shows, they disappear to become an reentrant planar orientation. The tubular orientation walls shown in Figure 4(i) form not by pinching of a pair of orientations walls, but directly from individual nucleation of non-planar orientation in the middle of the reentrant planar orientation field.

CONCLUSIONS

A cascade of complex orientation texture evolutions has been computed using the literature values of the experimentally measured Leslie coefficients and Frank elastic constants. Four different kinds of texture evolutions, all involved with non-planar orientation walls, have been presented. In the order of increaing level of E ranges, they give rise to i) monotonic twist out-of-shear plane texture, ii) alternating twist out-of-shear plane texture, iii) tubular orientation walls via pinching of a pair of orientational walls, and iv) tubular orientation walls via non-planar orienation nucleation out of the reentrant planar orientation.

References

[1] A. Elliott and E.J. Ambrose, *Discuss. Faraday Soc.*, **9**, 246 (1950).

[2] W.J. Toth and A.V. Tobolsky, *Polymer Letters*, **8**, 537 (1970).

[3] G. Kiss and R.S. Porter, *Mol. Cryst. Liq. Cryst.*, **60**, 267 (1980).

[4] M. Srinivasarao and G.C. Berry, *J. Rheology*, **35**, 379 (1991).

[5] R.G. Larson and D.W. Mead, *Liquid Crystals*, **12**, 751 (1992).

[6] X. Yan and M.M. Labes, *Macromolecules*, **27**, 7843 (1994).

[7] J. Wang and M.M. Labes, *Macromolecules*, **25**, 5790 (1992).

[8] W.H. Han and A.D. Rey, *Macromolecules*, **28**, 8401 (1995).

[9] P.G. de Gennes and J. Prost, *The physics of liquid crystals*, (Clarendon Press, Oxford, 1993).

[10] W.H. Han and A.D. Rey, *Phys. Rev. E*, **49**, 597 (1994).

[11] G. Srajer, S. Fraden, and R.B. Meyer, *Phys. Rev. A*, **39**, 4828 (1989).

[12] W.H. Han, Ph. D. Dissertation, McGill University (1995).